A novel design of multi-stable metastructures for energy dissipation

Zhang, Y.; Tichem, Marcel; van Keulen, Fred

DOI
10.1016/j.matdes.2021.110234

Publication date
2021

Document Version
Final published version

Published in
Materials and Design

Citation (APA)
Zhang, Y., Tichem, M., & van Keulen, F. (2021). A novel design of multi-stable metastructures for energy dissipation. *Materials and Design*, *212*, Article 110234. https://doi.org/10.1016/j.matdes.2021.110234

Materials & Design 212 (2021) 110234

Contents lists available at ScienceDirect

Materials & Design

journal homepage: www.elsevier.com/locate/matdes

A novel design of multi-stable metastructures for energy dissipation

Yong Zhang *, Marcel Tichem, Fred van Keulen

Department of Precision and Microsystems Engineering Delft University of Technology, Mekelweg 2, 2628 CD Delft, the Netherlands

HIGHLIGHTS

- Lattice and hollow beam designs enable multi-stable metastructures to enhance their energy dissipation capability.
- Enhanced structural bending stiffness is the key factor that contributes to the increase of critical loads and energy dissipation.
- Tuning the overall beam thickness could effectively lead to a stiffer mechanical response, but it will be impeded by local buckling.
- The proposed design strategy can be extended to shell structures for enhancing energy dissipation.

GRAPHICAL ABSTRACT

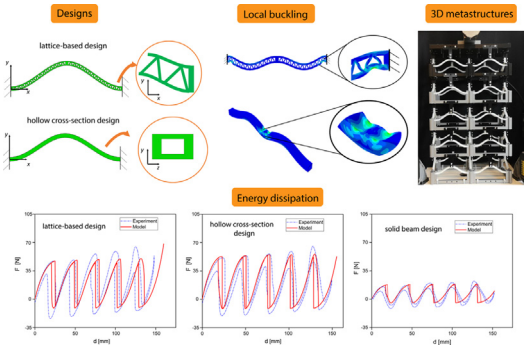

ARTICLE INFO

Article history:
Received 3 July 2021
Revised 4 November 2021
Accepted 7 November 2021
Available online 09 November 2021

Keywords:
Snap-through behavior
Multi-stable metastructure
Lattice structure
Cross-section design

ABSTRACT

Multi-stable metastructures composed of curved beams can switch to a series of stable configurations via elastic snap-through transitions. The elastic deformations allow metastructures to function as reusable energy absorbers. However, conventional metastructure designs based on solid beams often result in relatively low energy dissipation. In this work, it is found that by increasing the beam unit's bending stiffness while keeping the volume/mass constant, energy dissipation of the metastructure can be largely improved. Based on this observation, we propose two types of structural designs (lattice and hollow cross-section design) as building blocks for multi-stable metastructures. The lattice design is realized by incorporating lattice structures into pre-shaped beams while for the hollow cross-section design, a box-shaped cross section is adopted. The proposed structures are experimentally characterized under cyclic loading and are shown to exhibit sequential snap-through transitions with relatively large energy dissipation. Results show the snap-through behavior can be further tailored through tuning structural in-plane thickness. Effects of geometric parameters on snap-through, local buckling and bi-stability are investigated, and the feasible design domains for selecting proper lattice and cross-section geometries are identified. In addition, we demonstrate that the proposed design is not restricted to beams, and can be extended to shell structures.

1. Introduction

Energy absorping materials play important roles in protecting delicate objects and mitigating impact in many fields, for example, automobiles, aircraft and civil engineering [1]. To realize energy absorption, a number of strategies have been proposed to dissipate energy during a crash, including lightweight honeycomb structures [2,3], sandwich structures [4–6], and metallic foams [7,8]. The energy dissipation of these structures is mostly associated with plastic deformations and thus it results in inevitable structural damage.

* Corresponding author.
E-mail address: Y.Zhang-15@tudelft.nl (Y. Zhang).

https://doi.org/10.1016/j.matdes.2021.110234

Recently, owing to its potential of achieving energy absorption with elastic deformations, the concept of designing mechanical metastructures with snap-through behavior has been proposed and extensively studied [9,10]. Mechanical metastructures are rationally designed periodic structures that exhibit novel functionalities from their elementary structures rather than material properties. The snap-through property is a type of buckling behavior that causes a structure to "jump" from one configuration to the other when the applied load exceeds a critical value. To build metastructures exhibiting snap-through behavior, pre-shaped curved beams, as structural elements that exhibit snap-through behavior, have commonly been adopted [11,12]. For metastructures composed of a number of curved beams, a sequential snap-through behavior and negative stiffness can be observed in the quasi-static load–deflection curves [13]. Moreover, these metastructures often exhibit a series of stable deformed configurations and are, thus, referred to as multi-stable beam-type metastructures (MBMs) [14,15]. The multi-stability enables metastructures to retain their deformed configurations without the need for continuous external loading, facilitating motion- and energy-related functionalities [9]. For instance, it has been demonstrated that multi-stability can be utilized to design mechanical logic gates for Boolean computations [16]. With regard to energy absorption, the MBMs can realize an hysteresis loop under a quasi-static loading–unloading cycle, whereas energy is dissipated through a dynamic snap-through process [17–19]. Unlike structures which dissipate energy by means of plastic deformations, these metastructures undergo elastic deformations and the deformed structure can be fully reversed back to its initial configuration. As a result, these metastructures can be reused as shock absorbers multiple times. Moreover, the energy absorption is rate independent in the sense that when the external loading frequency is significantly lower than the metastructure's lowest eigenfrequency, the resulting hysteresis is hardly affected by the loading rate [20–22].

Many prototypes of MBMs have been demonstrated and studied in literature. Different geometries have been proposed, including planar [23–30], three-dimensional (3D) cylindrical [14,31,32], hexagonal [33,34] and cubic geometries [35–37]. For instance, Restrepo et al. [24] and Zhang et al. [38] investigated energy dissipation of multi-stable metastructures comprising curved beams arranged in one (1D) and two directions (2D). Hua et al. [31] extended the planar beams to spatial curved beams for developing cylinder-shape metastructures. Ha et al. [35] combined six curved beams into a 3D unit cell and presented a metastructure design for realizing energy absorption in three directions. While these previous studies focused on multi-stable metastructures under compressive loads, Sun et al. [25] presented a type of multi-stable structure consisting of two non-identical elements, to achieve energy absorption under tension.

For multi-stable metastructures consisting of snapping units, their energy dissipation capability is closely connected with the unit cells' snap-through behavior [24,39]. That is, snap-through units with stiffer mechanical responses will lead to an improvement of metastructures' energy dissipation. In the case of MBM, most previous studies have concentrated on using solid beam units to design metastructures. In this paper, we aim to develop new designs for MBMs to realize better energy dissipation than the solid beam designs. Specifically, it is found that by increasing the beam units' bending stiffness to a large extent, the corresponding metastructures can exhibit an improved energy dissipation. Based on this observation, we propose two types of snapping beams with enhanced bending stiffness as building blocks to construct metastructures. That is, for a planar design, lattice structures are introduced into the curved beam to obtain an hierarchical beam. Another strategy is to design hollow beams with box-shaped cross sections. Compared with previously studied solid beams, the proposed designs enable dissipation of more energy without using more material. Moreover, the proposed designs introduce additional design parameters, providing a larger design space to tune the snap-through features. In addition, this concept of increasing structural bending stiffness can be extended to shell structures.

The remainder of this paper is organized as follows. The working principle of the proposed design is firstly discussed in Section 2. The concept of lattice and cross-section designs is elaborated in Section 3, where the key geometric parameters are specified and categorized. Furthermore, the experimental and numerical approaches we used are discussed. Section 4 presents the mechanical properties of unit cells comprising hierarchical and hollow beams. The effect of geometric parameters on snap-through transition is explored. In Section 5, we investigate the deformation characteristics of multi-stable metastructures under cyclic loading. The energy dissipation is evaluated both experimentally and analytically. A quantitative comparison between the proposed and traditional designs is discussed. In Section 6, we demonstrate the potential of extending the proposed design to develop lattice-based shells. Conclusions are presented in Section 7.

2. Design principle

The structural design in this work is based on the pre-shaped curved solid beam, as illustrated in Fig. 1(a). The beam's geometry can be described as:

$$y(x) = \frac{H}{2}\left(1 - \cos\left(2\pi\frac{x}{L}\right)\right), \tag{1}$$

where H, L, T, B represent height, span, in-plane thickness and out-of-plane width of the beam, respectively. The effective bending and axial stiffness of the beam are denoted as EI/L^3 and EA/L, respectively. When a force (denoted as F) is applied at the center, as shown in Fig. 1(a), the beam can exhibit a snap-through transition and may reach the second stable state (curved dashed line). Here, the force–displacement ($F-d$) response of the beam is studied analytically. An approximate analytical model is adopted, based on the principle of mode superposition. It has been shown that the model can provide a good estimate of the snap-through transition [31,40,41]. Here, the first seven buckling modes are employed as a basis, and governing equations are derived on the basis of the minimum total potential energy principle (see Supporting Materials).

The resulting force–displacement curves obtained from the analytical analysis are shown in Fig. 1(b), where snap-through transitions of structures with different bending stiffness but the same cross-sectional area (A) are presented. During the displacement-controlled loading, two critical forces (denoted as F_{max} and F_{min}) are identified, and the structure exhibits a negative tangent stiffness after reaching F_{max}. It can be noted that when enlarging the structure's effective bending stiffness, both F_{max} and F_{min} increase, and the absolute value of the negative tangent stiffness increases as well. The effect of bending stiffness on the snap-through behavior indicates that when the axial stiffness of the structure is kept unchanged, increasing the bending stiffness can effectively result in a stiffer mechanical response.

Increasing the absolute values of F_{max} and F_{min} enables to enhance the energy dissipation. For a multi-stable metastructure consisting of serially arranged curved beams, an hysteresis can be realized under a displacement-controlled loading–unloading cycle [20,24]. Fig. 1(c) shows a three-beam system for which the displacement at the top is prescribed. Due to unavoidable imperfections in practice, the element with the smallest F_{max} becomes unstable first and will snap. As a result, a dynamic process is initiated, leading to dissipation of energy. This dissipated energy is

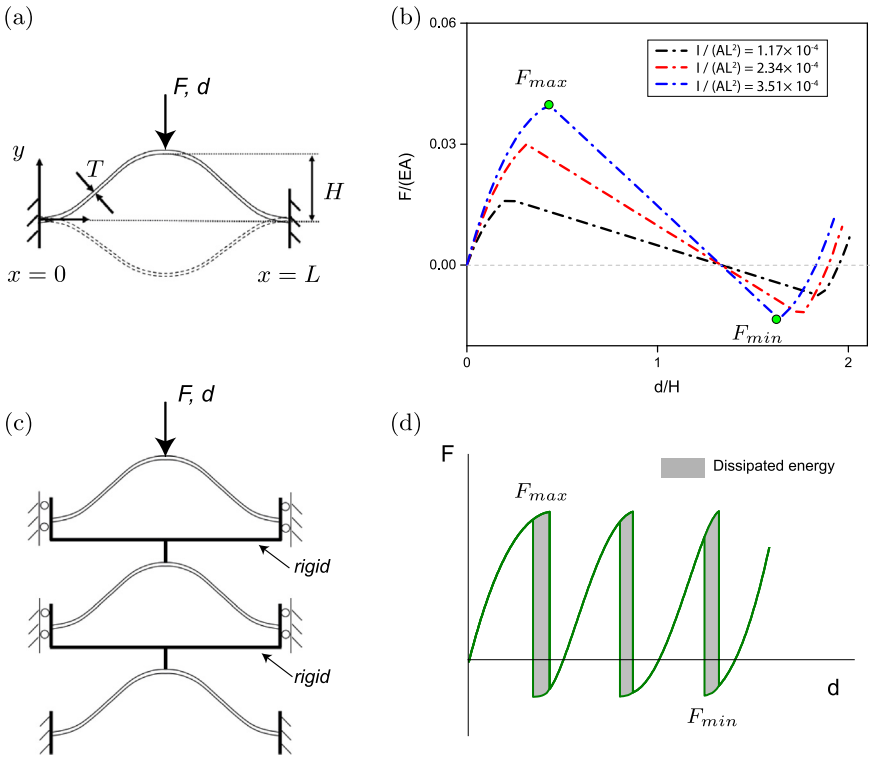

Fig. 1. Pre-shaped solid beams and the effect of bending stiffness on snap-through behavior. (a) A pre-shaped solid beam. The out-of-plane dimension is denoted as B. (b) The force–displacement curves predicted by the analytical model are shown, where cross-sectional area is kept as a constant value ($A = 12$ mm^2). Snap-through responses of beams with different relative bending stiffness are presented. (c) A system composed of three pre-shaped beams arranged in series. (d) The force–displacement curve of the three-beam system under a displacement-controlled loading cycle is illustrated.

converted to heat in turn. The other two beam units initially follow the stable unloading equilibrium without energy dissipation. Consequently, the corresponding force–displacement curve shows three "jumps" (see Fig. 1(d)). Similarly, for the unloading path, jumps will happen upon reaching F_{min}, resulting in the unstable transition of one element. After a loading–unloading cycle, an hysteresis loop, representing the energy dissipation of the metastructure, can be identified. It can be noted that the resulting hysteresis loop is closely associated with the beam unit's snap-through behavior. For the same amount of material, when adopting structural units with enhanced bending stiffness, it can be expected that better energy dissipation can be realized.

3. Structure design and methods

Following the concept of enlarging the relative bending stiffness, we present two types of structural design with improved energy dissipation. Note that the traditional solid beam whose geometry can be described by Eq. (1) is also studied for comparison, where H, T, L and B are referred to as global shape parameters.

3.1. Lattice design

The lattice design studied in this paper is focused on planar structures (x-y plane) that can be extruded along the out-of-plane (z) direction. As illustrated in Fig. 2(a), lattice structures (LSs) are incorporated into a pre-shaped beam to form a hierarchical beam. Similar to the solid beam, global shape of the hierarchical beam can be described by H, L, T and B (conform Eq. (1)). The distance between the top and bottom skin is denoted as T_v. The internal LS geometry can be described by two lattice parameters, i.e. t and θ, as depicted in Fig. 2(a). In addition, solid reinforcements with thickness D and $2D$ are introduced at the boundary and center, respectively (see Fig. 2(a)). The number of lattice cells (denoted as n_c) within the hierarchical beam is determined based on the following relation:

$$n_c = \text{int}\left[\frac{\int_0^L \sqrt{1+\left(\frac{dy}{dx}\right)^2}dx - 4D}{2T_v\tan(\theta)+\frac{2t}{\cos(\theta)}}\right] - 1, \tag{2}$$

where int represents a function that returns the integer part of a decimal number. Note that the hierarchical beam's mechanical properties are determined by a collective effect of the curved shape and the embedded lattices. As presented in Fig. 2(b), the designed hierarchical beam is then combined with rigid frames (in grey) to create a unit cell. By patterning such unit cells in 2D and 3D, multi-stable metastructures can be constructed accordingly (see Fig. 2(c)).

3.2. Hollow cross-section design

Next to the lattice-based design, we also investigate hollow beams with a box-shaped cross section, as presented in Fig. 2(d)–(f). It can be seen that in addition to the global shape parameters, the hollow beam has an internal cross section that can be described by b_1 and t_1 (see Fig. 2(d)). These curved beams with a box-shaped cross section are referred to as hollow beams in the remainder of this paper. The hollow beams are constructed by sweeping the box-shaped profile along the curved path (i.e. conform Eq. (1)). The associated 2D and 3D metastructures are demonstrated in Fig. 2(e) and (f).

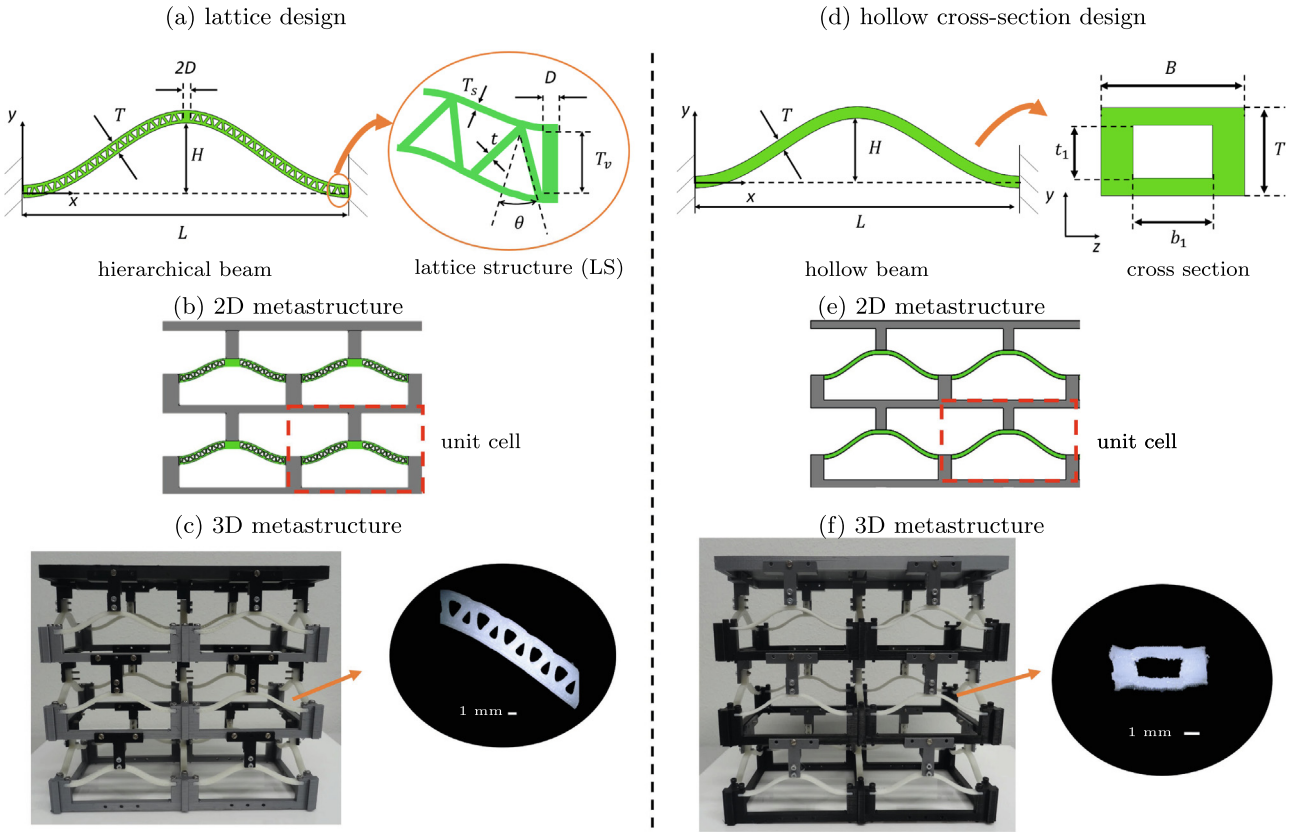

Fig. 2. A schematic of the proposed designs. (a)–(c): The developed lattice-based metastructures. Geometric parameters of the hierarchical beam are depicted in (a). (d)–(f): Metastructures based on hollow beams with box-shaped cross sections.

3.3. Fabrication and experiments

To experimentally evaluate the proposed structures, a series of samples is fabricated using fused deposition printing (Prusa i3-MK3 printer). The hierarchical, hollow and solid beams are printed with thermoplastic elastomers (Flex 98, RS), and frames are printed with a stiff material (polylactic acid, PLA). The beams and frames are assembled into unit cells by using screws. 3D multi-stable metastructures shown in Fig. 2(c) and (f) are built by assembling a series of unit cells. The material property of the elastomer is characterized by standard tensile measurements according to ASTM D638-14. The measured Young's modulus and Poisson's ratio are 87 MPa and 0.4, respectively.

Uniaxial loading tests are conducted to characterize the mechanical behavior. A displacement-controlled loading is applied using a universal testing system (ZwickRoell Z005). Specimens are loaded at the top with a crosshead speed of 10 mm/min, whereas the bottom edge of the specimen is fully clamped. The detailed information on the setup can be found in Supporting Materials.

3.4. Numerical simulations

To simulate the snap-through transition, finite element analysis (FEA) is carried out using ABAQUS (Standard, 2017). In the case of hierarchical beams, 2D structural models are constructed. Triangular and quadrilateral plane-stress elements (CPS3 and CPS4) are used. Mesh convergence tests have been conducted to ensure accuracy. Boundary conditions are assigned in such a way that the left and right end are fully constrained, and a vertical displacement is applied at the center. For the hollow beams, eight-node solid elements (C3D8) are employed. Using the measured Young's modulus and Poisson's ratio, a linear elastic constitutive relation is adopted.

In addition to quasi-static simulations, impact simulations are carried out to investigate the protective capabilities of the proposed metastructures. For this, we investigate the impact performance of metastructures using ABAQUS/Explicit. Based on the material properties of PLA and elastomers, the mass density of frames and beam elements are taken as 1240 kg/m^3 and 1140 kg/m^3, respectively. A rectangular object with a mass density of 7900 kg/m^3 is placed above the metastructure. The object has a Young's modulus of 210 GPa and a Poisson's ratio of 0.3. An initial velocity and a gravitational acceleration of 9.8 m/s^2 are introduced.

4. Mechanical behavior of unit cells

In this section, we investigate and present the mechanical properties of unit cells. The snap-through transitions are analyzed experimentally and numerically.

4.1. Snap-through behavior

Hierarchical, hollow and solid beams with the same volume (V) are constructed, and their geometric parameters are depicted in Table 1. It should be noted that H, L, and B of the hierarchical and hollow beam are the same for all beams, and are fixed throughout this study. In contrast, the hierarchical and hollow beam have a larger in-plane thickness T than the solid beam, which leads to an enhanced bending stiffness. Here, the unit cell's snap-through behavior is characterized experimentally and numerically. In the numerical model, 37314 elements are used for meshing the 2D

Table 1
Geometric parameters of unit cells.

	H [mm]	L [mm]	B [mm]	T [mm]	D [mm]	t/T_v	θ [°]	b_1/B	t_1/T	V [mm³]	bending stiffness [N/m]
hierarchical beam	16	80	6	2.55	1.0	0.4	25	\	\	999	1.13 [*]
hollow beam	16	80	6	2.55	\	\	\	0.53	0.50	999	1.29 [*]
solid beam	16	80	6	1.9	\	\	\	\	\	999	0.58

[*] The bending stiffness of the hierarchical and hollow beam is calculated using Eqn. (3) and (4), respectively.

hierarchical geometry. In case of the hollow beam, the geometry is modeled with 72314 solid elements. The measured and simulated force–displacement ($F-d$) curves are shown in Fig. 3(b), where the displacement (d) is normalized by H. It can be observed that the experimental and numerical results are in a good agreement, and all three configurations exhibit snap-through transitions. Upon loading, F gradually reaches the maximum force (denoted as F_{max}). As the displacement increases further, the tangent stiffness switches to a negative value until the minimum force (denoted as F_{min}) is reached. Next, the tangent stiffness becomes positive again and the deformed stable state (State 2) shown in Fig. 3(a) can be realized. After releasing the load, the unit cell can stabilize at the State 2. When compared with the solid beam, both the hierarchical and the hollow beam can realize larger F_{max} and F_{min} due to the enlarged bending stiffness. Note that for the hierarchical and hollow beam, it is possible to tune T while keeping the volume unchanged. This tuning of T may result in further increase of F_{max} and F_{min}, as studied in Section 4.2.

The enhanced bending stiffness causes the beam to deform into a stable state with an higher strain energy. Here, strain energy (P) of the unit cell is derived by calculating the integral of F with respect to d, as shown in Fig. 3(c). It can be seen that State 2 of each beam corresponds to a local minimum in the strain energy, which mainly consists of bending and compression energy. After removing the external load, the strain energy can be stored within the deformed state (i.e. energy trapping [15]). For the hierarchical and hollow beams, the enlarged bending stiffness enables the structure to store more bending energy within the deformed stable state, enhancing the structure's energy trapping capability.

4.2. Tuning of snap-through behavior

a. Hierarchical beams
For given H, L, and B, the hierarchical beam's bending stiffness can be further tuned by varying T, whereas the volume is kept constant. As noted in [42,43], the hierarchical beam's bending stiffness (D_l) can be approximated as:

$$D_l = \frac{EI_2}{L^3(1-\nu^2\frac{I_1}{I_1+I_2})}, \text{ with } I_1 = \frac{t(T_v)^3}{6\cos(\theta)},$$
$$I_2 = B\frac{T_s^3 + 3T_s(T_v+T_s)^2}{6}, \text{ and } T_s = \frac{T-T_v}{2}, \quad (3)$$

where E and ν represent Young's modulus and Poisson's ratio of the material, and T_s represents thickness of the skin (see Fig. 2(a)). From Eq. (3), it can be seen that changing lattice parameters (t and θ) has minor influence on the bending stiffness, whereas D_l can be effectively tuned by changing the in-plane thickness T. Thus, we study effects of T on the critical loads (F_{max} and F_{min}). Furthermore, it is worth mentioning that the hierarchical beam normally has lower axial stiffness than the solid beam with the same volume [42]. This is because the inclined lattice planes could not effectively bear the axial load, resulting in a reduction of their axial stiffness. Specifically, the thickness T is varied, while the volume is kept constant by adjusting t. Simulated and measured results are shown in Fig. 4(a), where F_{max} and F_{min} of the hierarchical beams are normalized by the counterpart of the solid beam. It can be seen that as compared to F_{min}, F_{max} is more sensitive to the change of the thickness. As T increases, it is possible to increase F_{max} to be two times as

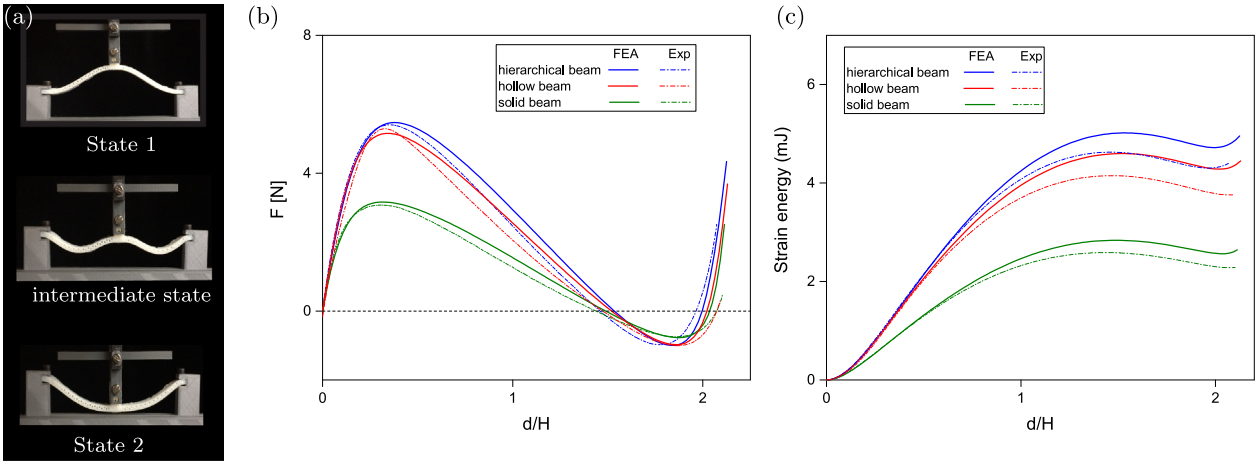

Fig. 3. Snap-through behavior of unit cells. (a) Snapshots of a hierarchical beam during the un-axial loading. (b) The measured and simulated force–displacement curves of the hierarchical, hollow and solid beams. (c) Evolution of the unit cell's strain energy during the uniaxial loading.

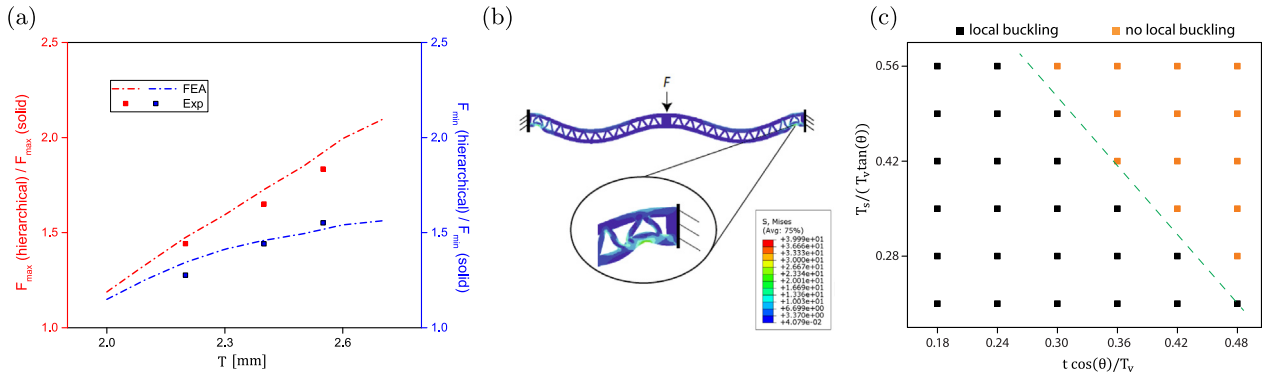

Fig. 4. Tuning the hierarchical beam's snap-through behavior via varying the thickness T. (a) Experimentally and numerically characterized critical loads as a function of T. (b) The local buckling. (c) Effect of the lattice parameters on the local buckling.

large as that of the solid beam. The increase of the critical load is mainly attributed to increasing of the bending stiffness. However, further increasing T will result in local buckling, which causes the strain and stress to increase dramatically at the local region. Here, the maximum strain reaches to 58%, which leads to plastic deformations and diminishes reversibility and reusability of the metastructures. Thus, it is important to select proper geometric parameters to avoid failure due to the local buckling. As shown in Fig. 4(a), when T is taken as 2.8 mm, local buckling happens for segments near the boundary (see Fig. 4(b)). This local buckling behavior is caused by the fact that under the constant volume constraint, increasing the thickness (T) leads to a decrease of the lattice thickness t. As a result, slenderness of the segment and the lattice are increased, making the structure prone to buckling.

To further explore the effect of the lattice parameters on the local buckling, a parametric study is carried out using finite element models. The corresponding results are shown in Fig. 4(c). In this figure, t and T_s are normalized by $\frac{T_v}{\cos(\theta)}$ and $T_v \tan(\theta)$, respectively. Orange dots represent that the hierarchical beam is able to snap into the second stable state without local buckling. Black dots indicate that local buckling behavior occurs. For relatively large t and T_s, the structure exhibits no local buckling. However, when t and T_s are reduced, the outer skin or the inner lattice become thinner, leading to local buckling. In order to achieve proper energy dissipation, it is important to ensure the lattice geometry to fall into the orange region.

b. Hollow beams

For hollow beams, the overall thickness T can also be tuned, whereas the volume is kept constant. Note that due to the volume constraint, the hollow beam has the same axial stiffness as that of the solid beam because they have the same cross-sectional area. Here, T of the hollow beam is varied and its influence on the critical loads is studied. When varying T, t_1 is adjusted subsequently for keeping the volume constant. In particular, the hollow beam's bending stiffness (D_h) can be expressed as:

$$D_h = \frac{1 - \frac{b_1}{B}\left(\frac{t_1}{T}\right)^3}{12L^3}(BT^3). \tag{4}$$

It can be noted from Eq. (4) that T has a dominant effect on D_h. Results presented in Fig. 5(a) verify that enlarging T can lead to an increase of both F_{max} and F_{min} when compared with the solid beam. Moreover, it can be observed that by tuning the thickness, F_{max} of the hollow beam can be two times larger than that of the solid beam. Although further increasing T can give rise to larger D_h, the snap-through transition will be suppressed by local buckling, similar to the hierarchical beam. For the hollow beam, as the volume is kept constant, increasing T causes t_1 to increase rapidly. Consequently, t_1/T increases at close to 1 and the hollow beams' walls become thinner. Effects of b_1/B and t_1/T on local buckling are studied numerically. From Fig. 5(b), it can be seen that when b_1/B or t_1/T is close to 1, local buckling occurs, as illustrated in Fig. 5(c). During the loading, the slender wall experiences high compressive stresses due to the bending as well as the axial compression. As a result, the hollow beam can not realize the second stable state. It can be expected that changing the thickness (T) offers the potential to further enhance the metastructure's energy dissipation, whereas it has to be constrained within a certain range to avoid local buckling.

4.3. Bi-stable behavior

Previous studies have shown that the ratio of the height to the thickness (H/T) is an important quantity for solid beams to realize bi-stable behavior [40,44]. When H/T of the solid beam is smaller than a certain value, the structure exhibits mono-stable behavior ($F_{min} > 0$). As compared to the solid beam, the hierarchical and the hollow beam have different geometric parameters, making their bi-stable criterion distinct from the solid beam. Here, bi-stability of the hierarchical and hollow beam is studied numerically.

For hierarchical beams, the lattice parameters (t and θ) have a minor influence on F_{min} because changing lattice parameters results in a small variation of the bending stiffness (see Eq. (3)). As a result, varying t and θ do not affect bi-stability much (see Supporting Materials). Based on this observation, we study the bi-stability criterion for hierarchical beams on the basis of two normalized quantities H/T and T_v/T, as presented in Fig. 6(a). In this figure, the yellow region indicates bi-stability ($F_{min} < 0$), while the grey area represents mono-stable behavior. The boundary corresponding to $F_{min} = 0$ is denoted as a red curve. Note that when T_v equals zero, it corresponds to the solid beam. Results show that the required H/T for the hierarchical beam to realize bi-stability is larger than that of the solid beam. Different from the solid beam, the hierarchical beam's bi-stability criterion is not only dependent on H/T, but also is influenced by T_v/T. When T_v increases, a larger H/T is required for achieving the second stable state. This happens because tuning T_v results in an evident change of the bending stiffness, which will affect F_{min} significantly.

In addition, the bi-stability criterion for hollow beams is investigated based on two normalized quantities H/T and t_1/T. From Fig. 6(b), it can be noted that for low values of H/T, the structure exhibits mono-stable behavior. The critical H/T corresponding to $F_{min} = 0$ (blue curve) increases as t_1/T increases. Therefore, when designing bi-stable hollow beams, both H and t_1 should be properly selected. Compared to the hierarchical beam, variation of the critical H/T for bi-stability is not significant. This is because the effect

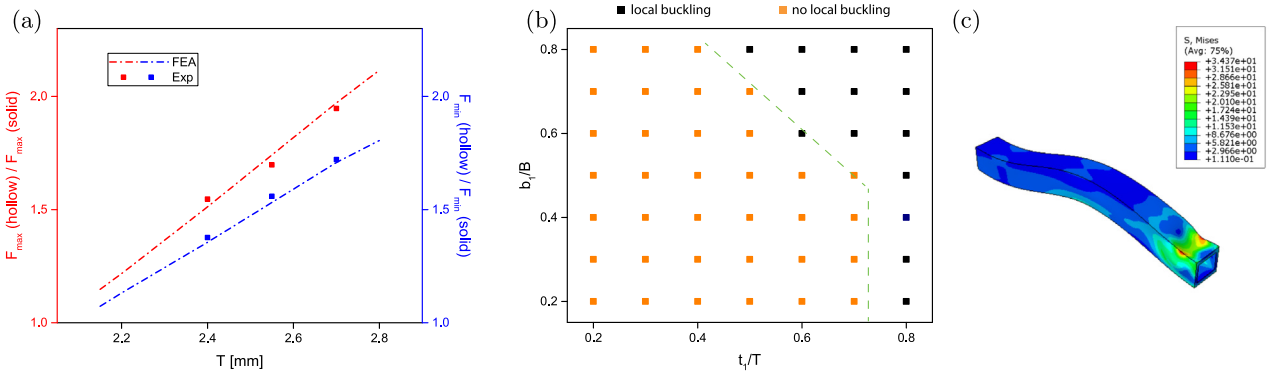

Fig. 5. Tuning the critical loads for the hollow beam. (a) Experimentally and numerically characterized critical loads are plotted as a function of T. (b) The effect of the inner cross-sectional parameters (b_1 and t_1) on local buckling. (c) The local buckling of the hollow beam.

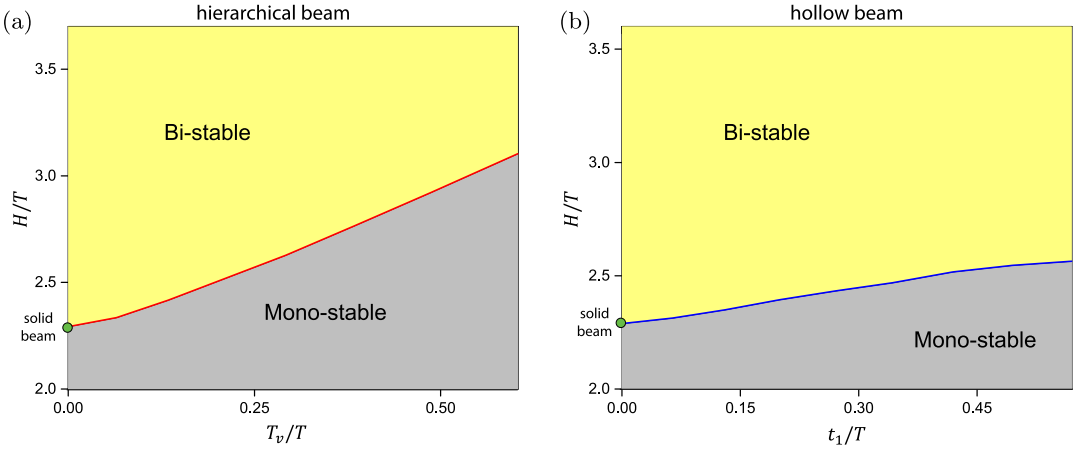

Fig. 6. The bi-stable criterion for the hierarchical and hollow beam. (a) With changing H/T and T_v/T, the bi-stable region for hierarchical beams can be identified. (b) For the hollow beam, the bi-stable region is plotted as a function of H/T and t_1/T.

of t_1 on the structural bending stiffness is not as evident as that of T_v (see Eq. (4)).

5. Multi-stable metastructures

In this section, the energy dissipation of metastructures is investigated. As discussed in Section 2, metastructures comprising a series of snap-through units can achieve energy dissipation such that the dissipated energy can be quantified as an hysteresis loop in the loading–unloading process. Here we analyze the metastructures' hysteresis characteristics and study their energy absorption capability. Note that the metastructures are formed by arranging the unit cells in three directions, leading to multiple stable configurations for the metastructures (see Fig. 7(a)). Due to inevitable manufacturing imperfections, units will exhibit slightly different critical loads, resulting in a sequential snap-through transition.

5.1. Energy absorption under a loading–unloading cycle

Based on the proposed lattice-based and hollow cross-section design, five-layer multi-stable metastructures are studied. Furthermore, metastructures consisting of solid beams (traditional design) are also fabricated. For the sake of simplicity, metastructures based on the lattice, hollow cross-section and traditional design are referred to as LM, HM, and TM, respectively, in the remainder of this paper. It should be noted that LM, HM, and TM have the same mass.

Cyclic loading tests are performed on each metastructure. Fig. 7 (a) shows different stages of the loading–unloading process of the LM. During loading, the snap-through sequence (i.e. which layer snaps first) is mainly determined by the inevitable manufacturing and assembly imperfections, which cause a sequential buckling from the weakest to the strongest layer. Measured force–displacement responses of the LM, HM and TM under a complete displacement-controlled loading–unloading cycle are denoted as blue dashed lines in Fig. 7(b)–(d). It can be seen that as the displacement increases, the slope of tangent lines, as highlighted in Fig. 7(b), increases. This is due to the fact that the stiffness of each layer's deformed state is larger than that of the initial state. As a result, when more layers flip into the deformed state, the effective tangent stiffness increases. Moreover, a force drop can be clearly observed when reaching F_{max}, in particular, for the LM and HM. That is, one layer jumps from one configuration to another with some mechanical energy dissipated to heat. Similarly, during the unloading process, when the minimum force is reached, the load increases suddenly, resulting in a configurational transformation. Consequently, an hysteresis can be identified, as displayed in the figures. It should be noted that the force drop also occurs for the TM (see Fig. 7(d)) even though it is not as evident as that of the LM and HM. In addition, force–displacement curves of the metastructures may be influenced by the polymer's cyclic softening, which will result in a reduction of critical loads after a few loading–unloading cycles [45]. Here, it is found that for the thermoplastic elastomer we used, the softening effect is small (see Supporting Materials).

Moreover, results shown in Fig. 7(b)–(d) indicate that for a given amount of material, the proposed lattice-based and hollow cross-section design can effectively give rise to a larger hysteresis

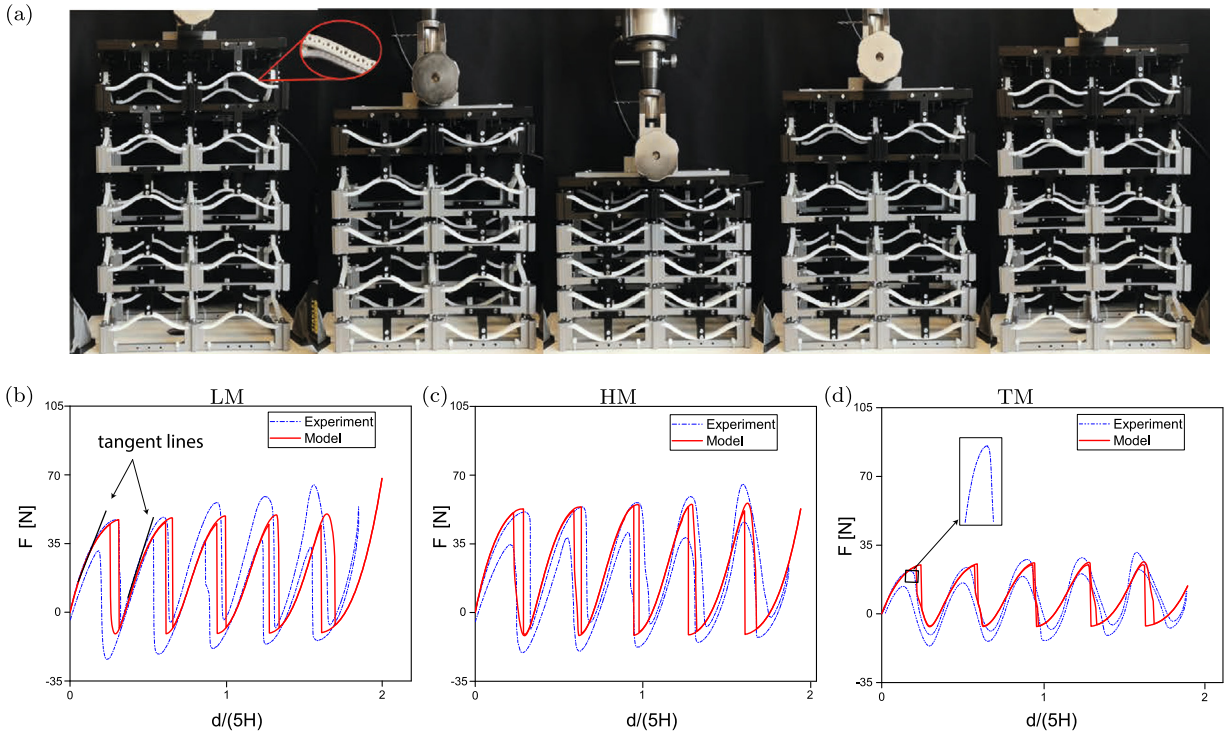

Fig. 7. Mechanical responses of multi-stable metastructures under displacement-controlled cyclic loading. (a) Different deformation stages of the LM in a loading–unloading test. (b)–(d) Force–displacement curves of the LM, HM, and TM under a complete displacement-controlled loading and unloading cycle.

loop (i.e. energy dissipation capability) when compared with the TM. The critical forces, in particular F_{max}, are significantly increased due to the enhanced bending stiffness. As discussed in Section 2, the increase of the bending stiffness generates higher critical forces, enhancing the energy absorption for multi-stable metastructures. As a result, evident and large hysteresis can be captured in the LM and HM.

In addition to the qualitative comparison, we also investigate the energy dissipation quantitatively. Specifically, an analytical calculation is carried out to predict the force–displacement response of n-layer metastructures. The analytical model is based on the following steps: i) the measured force–displacement curve of the unit cell is firstly fitted as a polynomial function $F(d)$. Next, the corresponding strain energy $P(d)$ is obtained by an integration of $F(d)$ with respect to d. ii) each layer of the n-layer metastructure is assumed as a structural element whose behavior is governed by $F(d)$ and $P(d)$. Hence, the metastructure possesses n degrees of freedom, which are defined as $(d_1, d_2, d_3 \dots d_n)$. Note that d_i represents deformation of the i-th layer. iii) in order to obtain the force–displacement curve, we solve the following optimization problem:

$$\begin{aligned} &\min_{d_i} E(d_1, d_2, d_3 \dots d_n) \\ &\text{subject to } d_1 + d_2 + d_3 \dots + d_n = d_{inp}, \end{aligned} \tag{5}$$

where $E(d_1, d_2, d_3 \dots d_n)$ is the strain energy of the n-layer metastructure, and d_{inp} is the prescribed displacement at the top of the metastructure. Once $(d_1, d_2, d_3 \dots d_n)$ are solved, the reaction force can be obtained by substituting one component d_i to compute $F(d_i)$. To ensure a sequential snapping deformation, we introduce imperfections by varying the critical loads of each layer by 0.5%. This optimization problem is solved using the fmincon interior-point algorithm implemented in Matlab. Calculated results are plotted as red lines in Fig. 7(b)–(d). From the figures, it can be seen that the model is able to capture the hysteresis loop caused by the snap-through transition associated with the force jump, well demonstrating the dynamic snapping as well as the energy dissipation. In addition, it is noted that there is a quantitative difference of dissipated energy between the experiments and models. That is, the area of the hysteresis loop in experiment is larger than that of the models, with differences in the range of 30%–50%. This discrepancy is caused by two factors: i) In experiments, apart from the dynamic snapping, the viscosity of polymers also contribute to the hysteresis loop, enlarging the dissipated energy. In the model, the viscous material damping is not taken into account as our focus is on the snap-through induced energy dissipation. It can be expected the error can be largely reduced when an appropriate visco-elastic constitutive relation is adopted; ii) Due to inevitable manufacturing imperfections, the beam units' mechanical properties (e.g, critical forces) are different even though they are designed to be identical. This also causes the difference between the experiments and models in terms of the amount of dissipated energy.

Using this model, we further investigate the relation between the energy dissipation and the number of layers. Force–displacement responses of metastructures with different amount (n) of layers are shown in Fig. 8(a). It can be seen that as n increases, more layers experience the force jump. Furthermore, it can be seen that the enclosed hysteresis for each jump (loading–unloading) becomes larger as n increases, leading to an increase of the energy dissipation of each layer [23,24]. For instance, compared to the 10-layer metastructure, an enlarged hysteresis can be observed for the 30-layer metastructure. When n becomes very large, the associated hysteresis will be enclosed by two straight lines at F_{max} and F_{min}, as illustrated in Fig. 8(a). In this case, each layer reaches its maximum energy dissipation capacity, which can be approximated as:

$$E_{max} \approx 2H(F_{max} - F_{min}), \tag{6}$$

where E_{max} is the maximal hysteresis area that can be achieved for each layer under a loading–unloading cycle (i.e. the area enclosed by the blue dashed curves in Fig. 8(a)). Therefore, in order to improve the energy absorption, it is important to increase the absolute value of both F_{max} and F_{min}.

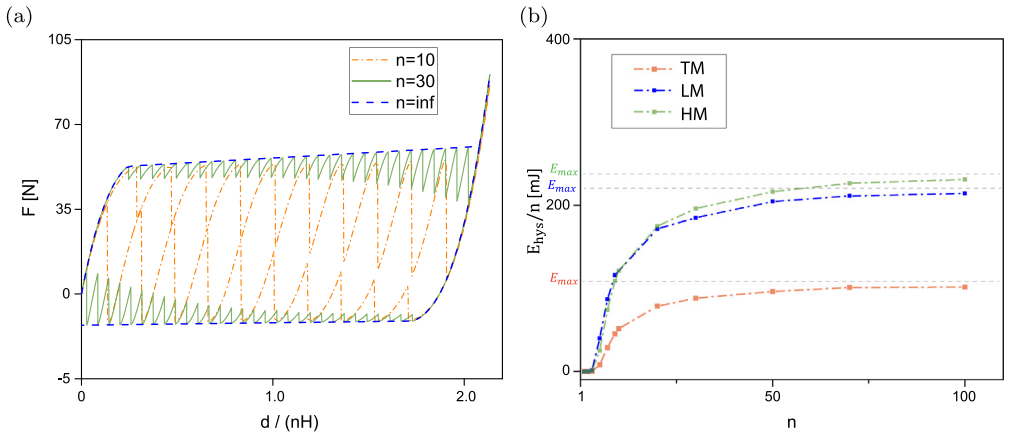

Fig. 8. Energy dissipation of n-layer metastructures. (a) The predicted force–displacement curves of n-layer metastructures. (b) The comparison between the LM, HM, and TM in terms of energy dissipation. E_{max} represents the maximal energy that can be dissipated per layer in a load-unloading process.

Fig. 8(b) presents quantitative comparison of the n-layer LM, HM, and TM in terms of energy dissipation. Here, area of the hysteresis loop (denoted as E_{hys}) is divided by n, which represents energy dissipation per layer. Results show that as n increases, there is a dramatic increase of E_{hys}/n. Further increasing n will cause E_{hys}/n to converge to the theoretical limit, namely E_{max} (see Fig. 8 (b)). Furthermore, it can be seen that the metastructure's energy dissipation can be largely enhanced by the proposed designs. Note

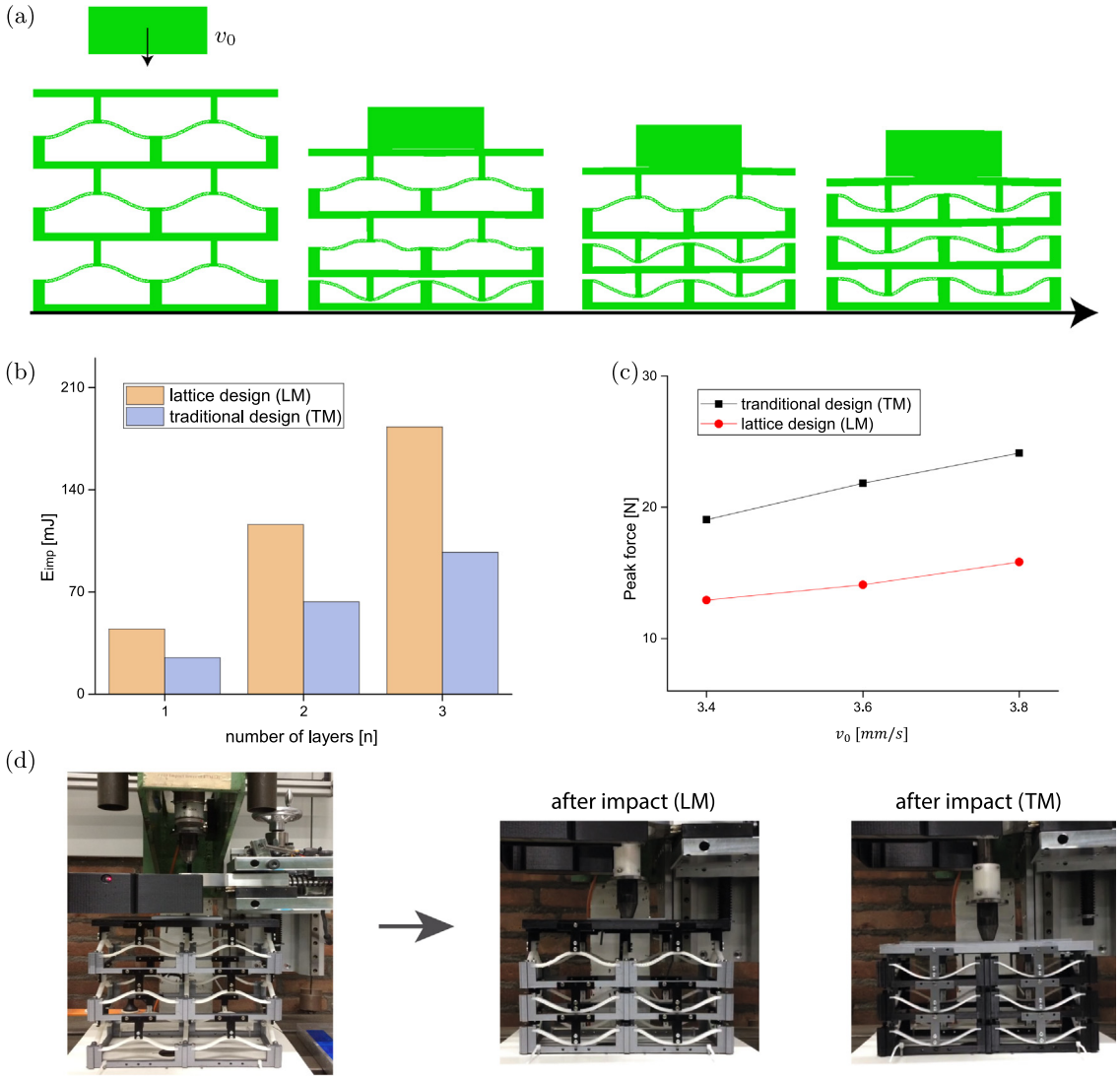

Fig. 9. Protective capability of multi-stable metastructures. (a) Different stages of metastructures' deformations under an impact. (b) The simulated critical mechanical energy (E_{imp}) of the LM and TM. (c) Simulated peak forces for the TM and LM design. (d) Experimental demonstration of the impact performance for the LM and TM.

that for the LM and HM, this enhancement can be further tuned by changing its in-plane thickness (T), whereas the total volume is kept constant. Therefore, as compared to TM, the proposed LM and HM offer a larger design space to tune the energy dissipation. It should be noted that in case of fabricating LM or HM with small features, more precise printing technique, like stereolithography (SLA), can be used. Apart from high resolutions, the SLA process also allows to print 3D metastructures directly without the manual assembly, simplifying the fabrication process.

5.2. Cushion performance of metastructures under impact

In addition to energy dissipation under quasi-static cyclic loading, multi-stable metastructures can also function as a buffer to protect an object from impact. To demonstrate this protective capability, here we study impact performance of the metastructures numerically. In particular, 2D structural geometries for the LM and TM are constructed, and the structural dimensions can be found in Table 1. Fig. 9(a) displays different stages of a three-layer LM's deformations under an impact load, for which an object with an initial velocity (v_0) drops from a certain height (h_0) above the metastructure. As shown in this figure, all three layers snap into the deformed state. Note that the number of snapped layers depends on the object's mechanical energy. The impact energy capacity (E_{imp}) for the multi-stable metastructure represents a critical mechanical energy that causes all layers to snap during the impact loading [15,46]. Here, a range of v_0 is given in the finite element models, and the impact energy is obtained by calculating the sum of the gravitational potential and kinetic energy of the object. It can be expected that as the impact energy increases, more layers will snap. In the numerical models, the critical impact energy that causes all layers to snap is monitored, namely E_{imp}. Results for multiple LMs and TMs with different layers are presented in Fig. 9(b). It can be seen that the introduced lattice is able to improve the structural cushion performance by means of sustaining a larger range of impact energy. Moreover, the impact force experienced by the ground is extracted from the simulations. Fig. 9(c) presents the peak force for the LM and TM design when different v_0 is taken. It can be seen that the proposed LM design leads to a smaller impact force compared to the TM, indicating better cushion performance in force mitigation. Since the LM exhibits similar snap-through response as the HM, it can be expected that the HM design can also enhance the structural impact performance when compared with the TM.

To demonstrate this improvement of cushion performance in practice, we perform a drop test using an in-house impact setup. As shown in Fig. 9(d), an impactor with a mass of 1.7 kg drops from a controlled height to the top surface of metastructures. Under the same initial height (160 mm), two layers of LM snap into the deformed state during the impact loading, whereas all three layers of the TM flip to the deformed state. This demonstrates that compared to the TM, the proposed designs enable metastructures to carry a larger range of impact loads with an enhanced cushion performance. The recorded video of the drop test is attached in Supporting Materials.

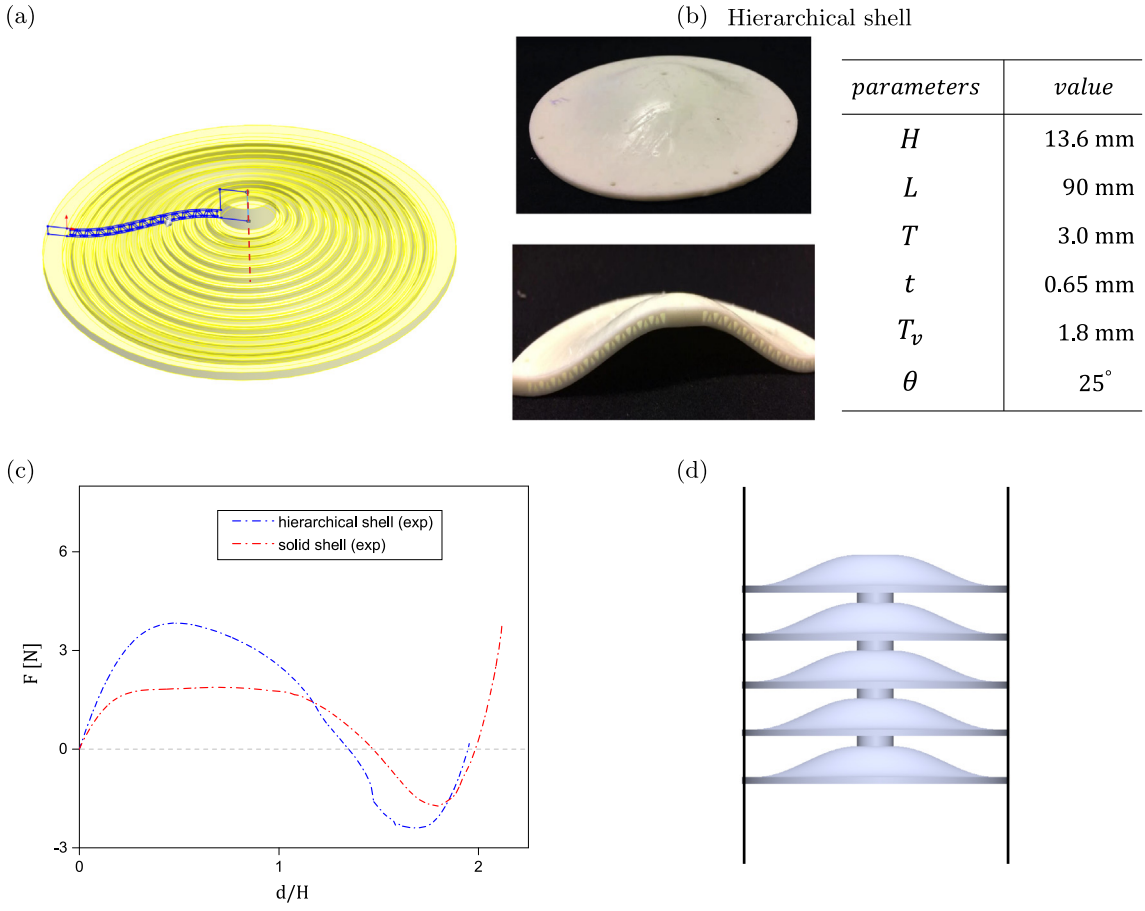

Fig. 10. The lattice-based shell structures. (a) The shell structure is developed by a revolution of the hierarchical beam profile (in blue) along the axis of rotation (red dashed line). (b) A real demonstration of the shell and its cross section. Geometric parameters are depicted. (c) The experimentally characterized force–displacement responses of the hierarchical and the solid shell. (d) An illustration of a serial arrangement of hierarchical shells for energy absorption.

6. Extension to shells

The proposed design strategy of increasing structural bending stiffness is not restricted to beams and can be extended to shell structures. In this section, we demonstrate this potential by developing a type of lattice-based shell with enhanced bending stiffness. As shown in Fig. 10(a), a shell structure can be constructed by a revolution of the 2D beam profile along the axis of rotation. Here, a lattice-based beam design is adopted, resulting in a hierarchical shell. A real demonstration of the shell structure fabricated with stereolithography printing (Prusa SL-1S) is presented in Fig. 10 (b). Dimensions of the associated hierarchical beam profile are shown in the inset table.

To demonstrate the improvement of mechanical response, we also fabricate solid shells with the same mass and conduct displacement-controlled loading tests. Measured force–displacement curves in Fig. 10(c) show that the hierarchical shell is able to enhance the snap-through transition in such a way that it exhibits larger critical loads than the solid shell. More importantly, it can be expected that when connecting multiple hierarchical shells in series, as illustrated in Fig. 10(d), the entire system is able to achieve a stiffer mechanical response than the previously reported structure that comprises a series of solid shells [47]. As a result, the energy dissipation capability of the shell structures can be effectively improved. The extension to shells here demonstrates generalization of the proposed concept, which can be used for enhancing energy dissipation of the solid shells. Although the lattice-based shell structure shows similarities with the hierarchical beam in terms of snap-through responses, its design space and energy absorption capability differ from that of the beam-type metastructures. Future research will be conducted to investigate energy dissipation of the hierarchical shells.

7. Conclusions

This paper presents a novel design of multi-stable metastructures with enhanced energy dissipation, based on the improvement of the structural bending stiffness. It is found that tuning the unit cells' bending stiffness while keeping the volume constant can result in a large benefit in terms of critical forces and energy dissipation. Two types of structural designs (the lattice-based and hollow cross-section design) are proposed for multi-stable metastructures. The snap-through transitions have been studied based on experimental and numerical approaches. Results show that snap-through transitions of the proposed structures can be further tuned by changing the beam thickness, leading to an effective tuning of the bending stiffness. Further increasing thickness will result in local buckling, which has been identified for the lattice-based and hollow cross-section design. Furthermore, it has been shown that as compared to metastructures consisting of solid beams, the proposed structures can lead to an improved energy dissipation by approximately a factor two. Moreover, the presented designs enable metastructures to sustain a larger impact energy with an enhanced impact performance. It has been demonstrated that the proposed strategy is not only applicable to beams, but also can be extended to shell structures. Our findings provide a new way to enhance the performance of multi-stable metastrutures for the application of energy absorption.

Supporting Materials

A. The detailed derivation for the snap-through behavior via the approximate analytical model.
B. The experimental setup of uni-axial loading.
C. The influence of lattice parameters on the bi-stable behavior.
D. Cyclic loading on metastructures.
E. Recorded videos for the LM and TM under impact loading.

Data availability

The raw/processed data required to reproduce these findings cannot be shared at this time as the data also forms part of an ongoing study.

Declaration of Competing Interest

The authors declare that they have no known competing financial interests or personal relationships that could have appeared to influence the work reported in this paper.

Acknowledgement

Y. Zhang would like to thank China Scholarship Council for the financial support. The authors thank Spiridon van Veldhoven and Patrick van Holst at Department of Precision and Microsystems Engineering of Delft University of Technology for their technical support.

Appendix A. Supplementary material

Supplementary data associated with this article can be found, in the online version, at https://doi.org/10.1016/j.matdes.2021.110234.

References

[1] J.C. Dixon, The Shock Absorber Handbook, John Wiley & Sons, 2008.
[2] C. Shen, G. Lu, T. Yu, Dynamic behavior of graded honeycombs–a finite element study, Compos. Struct. 98 (2013) 282–293.
[3] Z. Wang, Recent advances in novel metallic honeycomb structure, Compos. Part B: Eng. 166 (2019) 731–741.
[4] W. He, L. Yao, X. Meng, G. Sun, D. Xie, J. Liu, Effect of structural parameters on low-velocity impact behavior of aluminum honeycomb sandwich structures with CFRP face sheets, Thin-Walled Struct. 137 (2019) 411–432.
[5] G. Sun, D. Chen, X. Huo, G. Zheng, Q. Li, Experimental and numerical studies on indentation and perforation characteristics of honeycomb sandwich panels, Compos. Struct. 184 (2018) 110–124.
[6] G. Sun, X. Huo, D. Chen, Q. Li, Experimental and numerical study on honeycomb sandwich panels under bending and in-panel compression, Mater. Des. 133 (2017) 154–168.
[7] J. Shen, G. Lu, D. Ruan, Compressive behaviour of closed-cell aluminium foams at high strain rates, Compos. Part B: Eng. 41 (8) (2010) 678–685.
[8] M. Islam, M. Kader, P. Hazell, J. Escobedo, A. Brown, M. Saadatfar, Effects of impactor shape on the deformation and energy absorption of closed cell aluminium foams under low velocity impact, Mater. Des. 191 (2020) 108599.
[9] N. Hu, R. Burgueño, Buckling-induced smart applications: recent advances and trends, Smart Mater. Struct. 24 (6) (2015) 063001.
[10] K. Bertoldi, V. Vitelli, J. Christensen, M. van Hecke, Flexible mechanical metamaterials, Nature Rev. Mater. 2 (11) (2017) 17066.
[11] A. Rafsanjani, K. Bertoldi, A.R. Studart, Programming soft robots with flexible mechanical metamaterials, Sci. Robot.4 (29).
[12] H.Y. Jeong, S.-C. An, Y. Lim, M.J. Jeong, N. Kim, Y.C. Jun, 3D and 4D Printing of Multistable Structures, Appl. Sci. 10 (20) (2020) 7254.
[13] G. Simitses, D.H. Hodges, Fundamentals of Structural Stability, Butterworth-Heinemann, 2006.
[14] X. Tan, S. Chen, B. Wang, S. Zhu, L. Wu, Y. Sun, Design, fabrication, and characterization of multistable mechanical metamaterials for trapping energy, Extreme Mech. Lett. 28 (2019) 8–21.
[15] S. Shan, S.H. Kang, J.R. Raney, P. Wang, L. Fang, F. Candido, J.A. Lewis, K. Bertoldi, Multistable architected materials for trapping elastic strain energy, Adv. Mater. 27 (29) (2015) 4296–4301.
[16] Y. Song, R.M. Panas, S. Chizari, L.A. Shaw, J.A. Jackson, J.B. Hopkins, A.J. Pascall, Additively manufacturable micro-mechanical logic gates, Nature Commun. 10 (1) (2019) 1–6.
[17] D.M. Correa, T. Klatt, S. Cortes, M. Haberman, D. Kovar, C. Seepersad, Negative stiffness honeycombs for recoverable shock isolation, Rapid Prototyping J. 21 (2) (2015) 193–200.
[18] G. Puglisi, L. Truskinovsky, Mechanics of a discrete chain with bi-stable elements, J. Mech. Phys. Solids 48 (1) (2000) 1–27.
[19] R.C. Rogers, L. Truskinovsky, Discretization and hysteresis, Physica B 233 (4) (1997) 370–375.

[20] C. Findeisen, J. Hohe, M. Kadic, P. Gumbsch, Characteristics of mechanical metamaterials based on buckling elements, J. Mech. Phys. Solids 102 (2017) 151–164.
[21] G. Puglisi, L. Truskinovsky, Rate independent hysteresis in a bi-stable chain, J. Mech. Phys. Solids 50 (2) (2002) 165–187.
[22] I. Benichou, S. Givli, Structures undergoing discrete phase transformation, J. Mech. Phys. Solids 61 (1) (2013) 94–113.
[23] S. Liu, A.I. Azad, R. Burgueño, Architected materials for tailorable shear behavior with energy dissipation, Extreme Mech. Lett. 28 (2019) 1–7.
[24] D. Restrepo, N.D. Mankame, P.D. Zavattieri, Phase transforming cellular materials, Extreme Mech. Lett. 4 (2015) 52–60.
[25] S. Sun, N. An, G. Wang, M. Li, J. Zhou, Snap-back induced hysteresis in an elastic mechanical metamaterial under tension, Appl. Phys. Lett. 115 (9) (2019) 091901.
[26] H. Yang, L. Ma, Multi-stable mechanical metamaterials with shape-reconfiguration and zero Poisson's ratio, Mater. Des. 152 (2018) 181–190.
[27] D.A. Debeau, M.R. Haberman, Impact behavior of negative stiffness honeycomb materials, J. Mater. Res. 33 (3) (2018) 290–299.
[28] K. Che, C. Yuan, J. Wu, H.J. Qi, J. Meaud, Three-dimensional-printed multistable mechanical metamaterials with a deterministic deformation sequence, J. Appl. Mech. 84 (1) (2017) 011004.
[29] A. Rafsanjani, A. Akbarzadeh, D. Pasini, Snapping Mechanical Metamaterials under Tension, Adv. Mater. 27 (39) (2015) 5931–5935.
[30] T.A. Hewage, K.L. Alderson, A. Alderson, F. Scarpa, Double-Negative Mechanical Metamaterials Displaying Simultaneous Negative Stiffness and Negative Poisson's Ratio Properties, Adv. Mater. 28 (46) (2016) 10323–10332.
[31] J. Hua, H. Lei, Z. Zhang, C. Gao, D. Fang, Multistable cylindrical mechanical metastructures: Theoretical and experimental studies, J. Appl. Mech. (2019) 1–27.
[32] H. Yang, L. Ma, 1D and 2D snapping mechanical metamaterials with cylindrical topology, Int. J. Solids Struct. (2020).
[33] T. Frenzel, C. Findeisen, M. Kadic, P. Gumbsch, M. Wegener, Tailored Buckling Microlattices as Reusable Light-Weight Shock Absorbers, Adv. Mater. 28 (28) (2016) 5865–5870.
[34] Y. Zhang, Q. Wang, M. Tichem, F. van Keulen, Design and characterization of multi-stable mechanical metastructures with level and tilted stable configurations, Extreme Mech. Lett. 34 (2020) 100593.
[35] C.S. Ha, R.S. Lakes, M.E. Plesha, Cubic negative stiffness lattice structure for energy absorption: Numerical and experimental studies, Int. J. Solids Struct. 178 (2019) 127–135.
[36] C.S. Ha, R.S. Lakes, M.E. Plesha, Design, fabrication, and analysis of lattice exhibiting energy absorption via snap-through behavior, Mater. Des. 141 (2018) 426–437.
[37] C. Ren, D. Yang, H. Qin, Mechanical performance of multidirectional buckling-based negative stiffness metamaterials: an analytical and numerical study, Materials 11 (7) (2018) 1078.
[38] Y. Zhang, D. Restrepo, M. Velay-Lizancos, N.D. Mankame, P.D. Zavattieri, Energy dissipation in functionally two-dimensional phase transforming cellular materials, Sci. Rep. 9 (1) (2019) 1–11.
[39] B. Haghpanah, A. Shirazi, L. Salari-Sharif, A.G. Izard, L. Valdevit, Elastic architected materials with extreme damping capacity, Extreme Mech. Lett. 17 (2017) 56–61.
[40] J. Qiu, J.H. Lang, A.H. Slocum, A curved-beam bistable mechanism, J. Microelectromech. Syst. 13 (2) (2004) 137–146.
[41] Y. Zhang, M. Tichem, F. van Keulen, Rotational snap-through behavior of multi-stable beam-type metastructures, Int. J. Mech. Sci. 193 (2021) 106172.
[42] T.-S. Lok, Q.-H. Cheng, Elastic stiffness properties and behavior of truss-core sandwich panel, J. Struct. Eng. 126 (5) (2000) 552–559.
[43] D. Zangani, M. Robinson, A. Gibson, Evaluation of stiffness terms for z-cored sandwich panels, Appl. Compos. Mater. 14 (3) (2007) 159–175.
[44] J. Hua, H. Lei, C.-F. Gao, X. Guo, D. Fang, Parameters analysis and optimization of a typical multistable mechanical metamaterial, Extreme Mech. Lett. 35 (2020) 100640.
[45] A. Avanzini, D. Gallina, Effect of cyclic strain on the mechanical behavior of a thermoplastic polyurethane, J. Eng. Mater. Technol. 133 (2) (2011).
[46] F. Pan, Y. Li, Z. Li, J. Yang, B. Liu, Y. Chen, 3D Pixel Mechanical Metamaterials, Adv. Mater. 31 (25) (2019) 1900548.
[47] M. Alturki, R. Burgueño, Multistable Cosine-Curved Dome System for Elastic Energy Dissipation, J. Appl. Mech. 86 (9) (2019) 091002.